J. Plasma Phys. (2025), *vol*. 91, E47 © The Author(s), 2025. Published by Cambridge University Press.
This is an Open Access article, distributed under the terms of the Creative Commons Attribution licence (https://creativecommons.org/licenses/by/4.0/), which permits unrestricted re-use, distribution and reproduction, provided the original article is properly cited. doi:10.1017/S0022377825000182

Fresnel drag in a moving magnetised plasma

J. Langlois[1], A. Braud[1] and R. Gueroult[1]

[1]Université de Toulouse, CNRS, INPT, UPS, LAPLACE, Toulouse 31062, France

Corresponding author: J. Langlois, julien.langlois@laplace.univ-tlse.fr

(Received 7 June 2024; revision received 17 February 2025; accepted 18 February 2025)

The change in direction of the wavevector and group velocity experienced by a wave refracted at the interface of an anisotropic medium in uniform linear motion are determined analytically. These transmission conditions, which are shown to be consistent with the generalised Snell's law written in the laboratory frame, are then used to examine the effect of motion on waves incident on a magnetised plasma. For an incident wave in the plane perpendicular to the magnetic field the motion is observed to lead to non-negligible deviation of the low-frequency X-mode, as well as to non-symmetrical total reflection angles. These effects are shown to be further complicated when the magnetic field is in the plane formed by the incident wavevector and the medium's velocity, as the anisotropy now competes with the motion-induced drag. Although obtained in simplified configurations, these results suggest that accounting for motion when modelling plasma wave trajectories could be important under certain conditions, calling for a more detailed quantification of the effect of motion in actual diagnostics and plasma control schemes.

Keywords: Plasma waves, fusion plasma, plasma flows

1. Introduction

Wave propagation in moving media is affected by motion. Sorting out these effects, one may arrange the manifestations of motion in two groups. A first group gathers manifestations which manifest as 'phase' effects. One classical example is the modification of the phase index of a wave due to a motion of the medium along the wavevector, which materialises as the longitudinal Fresnel drag first postulated by Fresnel (1818) and later demonstrated by Fizeau (1851). Another example is the phase index difference between circularly polarised modes with opposite handedness introduced by a rotational motion, from which arises polarisation drag (Fermi 1923; Jones 1976; Player 1976). The second group gathers manifestations which manifest as 'ray' effects. An example is the modification of the group velocity that leads to the transverse drag or beam deflection experienced by a wave normally incident on a moving medium (Jones 1975; Player 1975; Carusotto *et al.* 2003).

While these effects have received considerable attention in isotropic dielectrics, notably since the realisation that drag effects can be enhanced in slow light

conditions (Franke-Arnold *et al.* 2011), the case of magnetised plasmas has been comparatively much less studied (Gueroult, Rax & Fisch 2023). On the other hand, because plasma waves are extensively used for plasma control and diagnostics, accurately modelling and quantifying the effect of motion on plasma waves are essential, and correcting for the generally neglected effect of motion might be of importance in a number of environments and applications. Information on the wave phase is for instance routinely used for diagnostics in the form of Faraday rotation measurements (Segre 1999; Van Eck *et al.* 2017), and it has recently been surmised that rotation corrections could have important implications for these measurements, notably in astrophysics. Specifically, interstellar magnetic field estimates are commonly inferred from pulsar polarimetry measurements that fail to account for polarisation drag in the rotating magnetosphere surrounding pulsars, and neglecting this effect has recently been shown to possibly lead to errors in magnetic field estimates (Gueroult *et al.* 2019). The effect of motion on the wave phase also creates opportunities to develop plasma-based non-reciprocal devices, which have been shown to hold high upside potential for light manipulation in the terahertz regime (Gueroult, Rax & Fisch 2020). As shown above though, the effect of motion is not limited to the wave phase: it can also affect the ray dynamics. It stands to reason that the effect of motion on these rays might be equally important. For instance, given that the effectiveness of cyclotron heating (Prater *et al.* 2008) and current drive (Fisch 1987) in tokamaks depends crucially on the accurate modelling of the propagation of radiofrequency waves across a moving plasma, it seems desirable to quantify what the effect of the plasma motion on radiofrequency beams is. Light drag is also fundamentally a manifestation of momentum coupling between the wave and the medium. Understanding how the ray dynamics in plasmas is affected by motion could thus bring insights into this basic yet important problem, notably in relation to the use of waves to drive rotation (Ochs & Fisch 2021*a*,b, 2022; Rax *et al*., 2023*b*,c,a; Ochs 2024). More generally, capturing the effects of motion on a plasma's response to a wave as seen by an observer in the laboratory frame is required to correctly determine wave accessibility in experiments featuring plasma flows. This is expected to be particularly relevant for fusion devices based on centrifugal confinement mechanisms (Lehnert 1971; Endrizzi *et al.* 2023; Kolmes *et al.* 2024), where one must know how a wave spectrum imposed by antennas outside the plasma is transmitted or not into the moving plasma, and can from there be used to effectively manipulate particles (Fetterman & Fisch 2008; Rubin *et al.* 2023, 2024). This may also create new means to maintain communications with a satellite reentering the Earth's atmosphere, by leveraging possible effects of motion to attenuate if not circumvent blackout (Rybak & Churchill 1971; Starkey 2015). Reversing finally the problem, determining accurately the effect of a moving plasma screen on the path of light between a distant source behind that screen and a static observer is expected to be important for a number of astrophysical applications. This has notably been shown to be true in the study of the physical properties of planetary atmospheres using time and frequency transfers in atmospheric occultation experiments (Bourgoin *et al.* 2019, 2021), where the assumption of an unmagnetised plasma made it possible to make use of Gordon's metric. It stands to reason that accounting for motion could prove just as important when using similar techniques to now determine the properties of magnetised plasma screens, such as a magnetosphere, or to model the effect of the said screen on the measured time of arrival of pulses from pulsars (Krishnakumar *et al.* 2021; Kumar *et al.* 2022).

https://doi.org/10.1017/S0022377825000182 Published online by Cambridge University Press

A challenge in determining the transverse drag that light incident on a moving magnetised plasma experiences is that magnetised plasmas are anisotropic media. For an observer in the laboratory frame this moving anisotropic medium then appears bianisotropic (Kong 1974, 2008). This difference makes the analysis of refraction at a moving interface, and thus of transverse drag, more involved than in isotropic media (Player 1975; Carusotto *et al.* 2003). In particular, one in general has to deal with two refracted beams which are each characterised by a group velocity $\mathbf{v}_g$ that is at an angle to the propagation direction $\mathbf{k}$. To avoid this complexity, a number of studies on transverse drag in plasmas have examined particular configurations – i.e. directions of the wavevector $\mathbf{k}$, the background magnetic field $\mathbf{B}_0$ and the medium velocity $\mathbf{v}$ – for which $\mathbf{v}_g$ and $\mathbf{k}$ are aligned even if the medium is anisotropic (Mukherjee 1975; Meyer-Vernet 1980). This is reminiscent of the fact that, although the dielectric tensor of a cold magnetised plasma is anisotropic, propagation parallel or perpendicular to the background magnetic field ($\mathbf{k} \parallel \mathbf{B}_0$ or $\mathbf{k} \perp \mathbf{B}_0$) is characterised by a group velocity aligned with the wavevector $\mathbf{v}_g \parallel \mathbf{k}$ (Ginzburg 1964, p. 145). In doing so the phase index of the mode does not depend on the direction of propagation, which as we will show simplifies substantially the derivation of the beam deflection angle. Yet, one expects that the geometry in actual applications will, at least locally, not match these simplified configurations, motivating the development of a more general theory.

In this paper we address this problem by constructing a general theory for refraction at the interface with an anisotropic medium in uniform linear motion, which we use to derive a formula for the transverse drag experienced by a wave at oblique incidence on this medium. In § 2, we begin by recalling the theory and manifestations of Fresnel drag at the interface with a moving isotropic medium. Then, in § 3, we extend this theory to the case where the moving medium is anisotropic, and briefly show in § 4 how the obtained drag coefficients can be seen as generalised Snell's laws written in the laboratory frame. We finally apply in § 5 these new results to the case of a moving magnetised plasma, showing that drag effects could be important, especially at low frequency, and also compete with the plasma anisotropy. Section 6 summarises the main findings of this study.

2. Fresnel drag in isotropic media

As a primer for the upcoming derivation in § 3 of drag in moving anisotropic media, we first recall in this section the theory of drag in moving isotropic dispersive media.

A derivation of the drag experienced by an electromagnetic wave refracted at the interface of a moving isotropic dispersive medium, generally referred to as Fresnel drag, was first proposed by Player (1975), and soon after that discussed in the particular case of a plasma by Ko & Chuang (1978). The central point of this derivation is, as we will show, to apply Snell's law of refraction in the frame of reference in which the interface between the medium and vacuum is at rest, using relativistic kinematics arguments to rewrite variables observed in the laboratory frame in terms of these same variables written in the rest frame of the interface. Note that because we restrict ourselves in this study to a medium in rigid-body motion, the rest frame of the interface is in fact the medium rest frame. We also consider here for simplicity a wave incident on a moving medium from vacuum, but note that the generalisation to the case of an incident wave propagating in a material medium at rest in the laboratory frame is straightforward. Lastly, when used with vector quantities the

https://doi.org/10.1017/S0022377825000182 Published online by Cambridge University Press

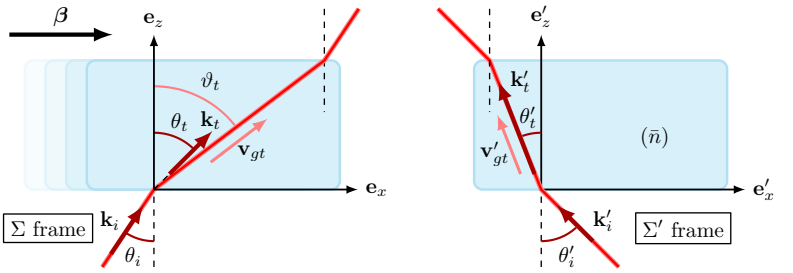


FIGURE 1. Light drag experienced by a wave at oblique incidence, as observed in the laboratory frame Σ (left) and in the medium's rest frame Σ' (right). Here the moving medium is isotropic at rest, so that the group velocity and the wavevector are aligned in Σ'. On the other hand, because they do not follow the same transformation rules from one frame to the other, they are misaligned in Σ.

adjectives normal, longitudinal and parallel (and tangential, transverse and perpendicular) are used throughout this paper to indicate projections along (and in the plane perpendicular to) respectively the interface normal, the wavevector and the magnetic field.

2.1. *Relations at the interface for a moving isotropic medium*

Consider a medium in uniform linear motion with velocity $\mathbf{v} = v\hat{\mathbf{x}}$ as seen in the inertial reference frame of the laboratory Σ. In its rest frame Σ' – which is also inertial since $\mathbf{v}$ is uniform – the medium is assumed to be homogeneous, isotropic and time dispersive. We note $\bar{n}(\omega')$ its optical index. The laboratory-frame coordinate system is chosen so that the interface between this moving medium (half-space $z > 0$) and the vacuum (half-space $z < 0$) defines the $(O, \hat{\mathbf{x}}, \hat{\mathbf{y}})$ plane, that is, that the medium moves parallel to its boundaries.

Consider now as illustrated on the left-hand side of figure 1 an electromagnetic, monochromatic wave with angular frequency ω in Σ incident from the vacuum onto the moving medium. We take for simplicity this wave to be in the $(O, \hat{\mathbf{x}}, \hat{\mathbf{z}})$ plane and accordingly write its wavevector $\mathbf{k}_i = (k_i^x, 0, k_i^z)$, though a generalisation to a non-zero k_i^y poses no particular problem. The angle of incidence relative to the surface normal $\hat{\mathbf{z}}$ in Σ is written θ_i. We would like to determine the properties of the refracted wave as seen in the laboratory frame Σ. To do so we will first consider refraction as seen in Σ'.

To obtain the incident wave properties in Σ' we use the fact that $(\omega/c, \mathbf{k})$ forms the 4-wavevector in Minkowski coordinates. Its transformation to Σ' is thus given by the Lorentz transformation (Einstein 1905; Landau & Lifschits 1975, p. 125):

$$\omega' = \gamma(\omega - k^x v), \tag{2.1a}$$

$$\Lambda: \quad k^{x\prime} = \gamma\left(k^x - v\omega/c^2\right), \tag{2.1b}$$

$$k^{z\prime} = k^z, \tag{2.1c}$$

where $\gamma = [1 - \beta^2]^{-1/2}$ is the Lorentz factor with $\beta = v/c$. In vacuum, $kc = \omega$ and one immediately finds

https://doi.org/10.1017/S0022377825000182 Published online by Cambridge University Press

$$\omega' = \gamma\omega(1 - \beta \sin\theta_i), \tag{2.2a}$$

$$k_i^{x'} = \gamma\omega\,(\sin\theta_i - \beta)\,/c, \tag{2.2b}$$

$$k_i^{z'} = \omega\cos\theta_i/c. \tag{2.2c}$$

Since the medium's boundaries are at rest in Σ', the spatial and temporal phase-matching conditions of Snell's law ($\mathcal{S}'$) must apply in Σ' at the interface ($z = 0$) (Player 1975). Using (2.2), one finds

$$\omega_t' = \omega', \tag{2.3a}$$

$$k_t^{x'} = k_i^{x'} = \gamma\omega\,(\sin\theta_i - \beta)\,/c. \tag{2.3b}$$

Here and throughout this study we denote respectively with indexes r and t reflected and transmitted wave variables. Equation (2.3b) provides the tangential part of the rest-frame transmitted wavevector. Meanwhile, the normal part may be determined from the definition of the optical index, that is,

$$\bar{n}(\omega') \overset{\text{def}}{=} \frac{c}{\omega'}\sqrt{k_t^{x'2} + k_t^{z'2}}. \tag{2.4}$$

With the refracted wavevector $\mathbf{k}_t'$ in hand we can now simply use the inverse Lorentz transformation (Λ^{-1}):

$$\omega = \gamma(\omega' + k^{x'}v), \tag{2.5a}$$

$$\Lambda^{-1}: \quad k^x = \gamma(k^{x'} + v\omega'/c^2), \tag{2.5b}$$

$$k^z = k^{z'}, \tag{2.5c}$$

to obtain from (2.3)–(2.4) the laboratory-frame transmitted 4-wavevector:

$$\omega_t = \omega, \tag{2.6a}$$

$$k_t^x = k_i^x = \omega\sin\theta_i/c, \tag{2.6b}$$

$$k_t^z = k_t^{z'} = (\gamma\omega/c)\sqrt{\bar{n}^2(1 - \beta\sin\theta_i)^2 - (\sin\theta_i - \beta)^2}. \tag{2.6c}$$

On the other hand, determining the refracted wave group velocity in Σ requires a little more work. One can, however, take advantage here of the fact that the phase and group velocity must be collinear in Σ', as the medium is isotropic. Specifically, one can write $\mathbf{v}_{gt}' = (c/\bar{n}_g)\hat{\mathbf{k}}_t'$ with $\bar{n}_g = \bar{n} + \omega' d\bar{n}/d\omega'$ the medium's rest-frame group index and $\hat{\mathbf{k}}_t'$ the unit vector along $\mathbf{k}_t'$. Then, since the group velocity transforms between inertial frames like particle velocities, the Einstein velocity addition theorem (Einstein 1905) can be used to give

$$v_{gt}^x = \frac{v_{gt}^{x'} + v}{1 + \beta v_{gt}^{x'}/c} = c\frac{k_t^{x'} + \bar{n}_g\sqrt{k_t^{x'2} + k_t^{z'2}}}{\beta k_t^{x'} + \bar{n}_g\sqrt{k_t^{x'2} + k_t^{z'2}}} \tag{2.7a}$$

and

$$v_{gt}^z = \frac{1}{\gamma}\frac{v_{gt}^{z'}}{1 + \beta v_{gt}^{x'}/c} = \frac{c}{\gamma}\frac{k_t^{z'}}{\beta k_t^{x'} + \bar{n}_g\sqrt{k_t^{x'2} + k_t^{z'2}}}. \tag{2.7b}$$

https://doi.org/10.1017/S0022377825000182 Published online by Cambridge University Press

It is worth noting that using the same approach to derive the phase velocity in Σ from its expression in Σ' would lead to a different (an erroneous) expression compared with what is given by (2.6) and the definition $\mathbf{v}_{\phi t} = \omega/\mathbf{k}_t$. This is simply because the phase velocity is not the spatial part of a 4-vector (Deck-Léger *et al.* 2021).

Putting these pieces together, we can finally derive the angle of refraction of the wavevector θ_t and of the ray ϑ_t shown in figure 1, which from (2.3)–(2.4) and (2.6)–(2.7) respectively are written

$$\tan\theta_t \overset{\text{def}}{=} \frac{k_t^x}{k_t^z} = \frac{\sin\theta_i}{\gamma\sqrt{\bar{n}^2(1-\beta\sin\theta_i)^2 - (\sin\theta_i - \beta)^2}} \tag{2.8}$$

and

$$\tan\vartheta_t \overset{\text{def}}{=} \frac{v_{gt}^x}{v_{gt}^z} = \gamma\frac{\bar{n}\bar{n}_g\beta(1-\beta\sin\theta_i) + (\sin\theta_i - \beta)}{\sqrt{\bar{n}^2(1-\beta\sin\theta_i)^2 - (\sin\theta_i - \beta)^2}}, \tag{2.9}$$

where both $\bar{n}$ and $\bar{n}_g$ are evaluated in $\omega' = \gamma\omega(1-\beta\sin\theta_i)$. We verify that (2.8) and (2.9) are consistent with the results derived by Ko & Chuang (1978). One further recovers the results of Player (1975) in the particular case of normal incidence $\theta_i = 0$. Finally these results are consistent with those of Gjurchinovski (2004) in the limit of a non-dispersive medium, i.e. for $\bar{n}_g = \bar{n}$.

An analogous, albeit simpler, treatment of the reflected wave shows that $\theta_r = \theta_i$, i.e. the reflection angle must always be equal to the incidence angle.

2.2. *Refraction diagram*

Having derived expressions for the refraction angle (2.8) and for the beam deviation angle (2.9), we now would like to provide some physical insights into these manifestations. To do so we consider here the particular and simpler case of a non-dispersive medium. The added contribution of dispersion is examined when discussing plasmas in § 5.

To discuss the origin of drag manifestations, we use the refraction diagrams shown in figure 2. These diagrams, in plotting the dispersion relation in (n_t^x, n_t^z) space, are similar to the isofrequency diagrams used for instance by Deck-Léger *et al*. (2021), though in our case these diagrams further incorporate the physics of refraction at the interface. To each incident vector corresponds a point on the unit half-circle that represents propagation in vacuum. From there conservation of the tangential wavevector component k_i^x at the interface can be used to immediately deduce the wavevector component along the surface normal k_t^z. The refracted wave group velocity is then aligned with the normal to the dispersion curve at this point, whereas the phase velocity is aligned with the orthoradial direction. To underline the effect of motion, we consider in figure 2 these diagrams in both Σ and Σ'.

In Σ' our moving medium is isotropic, so that the dispersion curve in $(n_t^{x'}, n_t^{z'})$ is also a half-circle, with radius $\bar{n}$. Equivalently the phase and group velocity are aligned, as expected for an isotropic medium. This is illustrated in the refraction diagrams on the right-hand side of figure 2. In contrast, we see moving to the refraction diagrams on the left-hand side of figure 2 that the dispersion curve in (n_t^x, n_t^z) is distorted. This is the effect of motion. One finds in particular that the dispersion curve is no longer a half-circle, and is notably asymmetrical with respect to k_i^x. As a result there is now a deviation between the phase and group velocity. This is light dragging induced by motion.

https://doi.org/10.1017/S0022377825000182 Published online by Cambridge University Press

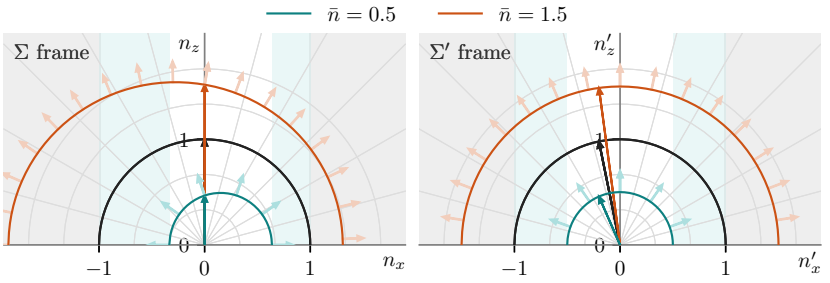


FIGURE 2. Refraction diagrams for a moving isotropic non-dispersive medium ($\beta = 0.2$) for two values of the rest-frame refractive index $\bar{n}$. The left-hand diagram corresponds to the laboratory frame Σ, whereas the right-hand diagram corresponds to the rest frame Σ'. The solid black line represents the vacuum dispersion curve for the incident wave. The solid coloured lines represent the moving medium dispersion curves ($\bar{n} > 1$ in red and $\bar{n} < 1$ in green). The long black and green/red arrows illustrate the incident and refracted wavevectors, respectively, for the particular case of normal incidence. The short green and red arrows on the dispersion curve represent the direction of the group velocity for the local wavevector.

Trying to shed light onto the origins of these manifestations, a contribution to the distortion of the dispersion curve going from Σ' to Σ is the misalignment between the wavevectors expressed in these two frames. The latter is itself a result of relativistic aberration, as can be seen in the Lorentz transformation (2.1). Specifically, since we find Snell's laws to take their usual form in the rest frame Σ', the incident wavevector for which a symmetrical dispersion curve is found is $\mathbf{k}'_i$, which is not aligned with $\mathbf{k}_i$ as the relative motion introduces a change of the component along the motion direction. This misalignment carries back to Σ' through the inverse Lorentz transformation written for $\mathbf{k}'_t$, giving the dispersion curve in (n_t^x, n_t^z) space an asymmetrical shape.

Finally, another facet of this motion-induced asymmetry is the shift of the critical angles above which total reflection occurs, as can be seen on the left-hand side of figure 2 for $\bar{n} < 1$. For an isotropic medium at rest, the total reflection critical angles are symmetrical $\pm\theta_i^{c\prime}$. This property comes naturally on the right-hand side of figure 2 as the dispersion curve in Σ' is again a half-circle centred on the origin. However, we verify on the left-hand side of figure 2 that the shift of the dispersion curve due to the motion leads to total reflection critical angles that are no longer symmetrical.

3. Refraction laws for an anisotropic dispersive medium in uniform linear motion

Having reviewed in the previous section the main traits of Fresnel drag in a moving isotropic medium, we can now examine how these results generalise to the case of an anisotropic medium. The major modification introduced by the medium's material anisotropy lies in the loss of the collinearity between phase and group velocities in the rest frame Σ', which as we have shown above was an essential argument in determining interface relations for the moving isotropic medium. An added complexity is that an anisotropic medium supports several propagation modes (denoted by an index α here), so that a monochromatic incident ray is refracted into as many rays as there are modes.

https://doi.org/10.1017/S0022377825000182 Published online by Cambridge University Press

Our starting point is the dispersion function for the mode α in the medium at rest, which we write here in generality as

$$\mathcal{D}'_\alpha\left(\omega', \mathbf{k}'\right) = \bar{n}_\alpha\left(\omega', \hat{\mathbf{k}}'\right) - k'c/\omega'. \tag{3.1}$$

We underline here that, importantly and unlike the isotropic case, $\bar{n}_\alpha$ is now a function of the direction of the wavevector $\hat{\mathbf{k}}'$. The dispersion functions of the different modes then yield the dispersion relation

$$\prod_\alpha \mathcal{D}'_\alpha\left(\omega', \mathbf{k}'\right) = 0. \tag{3.2}$$

The dispersion relation (3.2) is classically used to determine ω' for a given $\mathbf{k}'$, or vice versa. Here, however, we have seen in (2.3) that the continuity conditions at the interface impose $\omega' = \gamma\omega(1 - \beta\sin\theta_i)$ and $k_t^{x'} = \gamma\omega(\sin\theta_i - \beta)/c$. The dispersion relation (3.2) is then instead used to recast (3.1) as an implicit equation $\mathcal{D}'_\alpha\left(\omega', k_t^{x'}, k_{t\alpha}^{z'}\right) = 0$ for the normal component of the refracted wavevector $k_{t\alpha}^{z'}$ as a function of the tangential component of the refracted wavevector $k_t^{x'}$ and the rest-frame frequency ω', which we write

$$k_{t\alpha}^{z'} \overset{\text{def}}{=} \mathcal{K}'_\alpha(\omega', k_t^{x'}). \tag{3.3}$$

In other words,

$$\mathcal{D}'_\alpha\left(\omega', k_t^{x'}, \mathcal{K}'_\alpha(\omega', k_t^{x'})\right) = 0. \tag{3.4}$$

One further verifies that the inverse Lorentz transformation (2.5) does not affect this wavevector component, that is to say $k_{t\alpha}^{z} = k_{t\alpha}^{z'}$, which gives

$$k_{t\alpha}^{z} = \mathcal{K}'_\alpha(\omega', k_t^{x'}). \tag{3.5}$$

Equipped with the tangential and normal laboratory-frame wavevector components (2.6*b*) and (3.5), respectively, and the Doppler-shifted frequency (2.2*a*), the laboratory-frame transmitted phase angle (2.8) is written

$$\tan\theta_{t\alpha} = \frac{\omega\sin\theta_i}{c\mathcal{K}'_\alpha\left(\omega', k_t^{x'}\right)}. \tag{3.6}$$

We stress that ω' and $k_t^{x'}$ in (3.6) are not free variables but instead known functions of the laboratory-frame incident angle θ_i and the laboratory-frame wave frequency ω through (2.6*b*) and (2.2*a*).

Considering now the group velocity of the refracted wave, we can no longer take advantage of the alignment of the phase and group velocities in the rest frame Σ' used above for isotropic media. Instead we use here the definition (2.9) together with the inverse Lorentz transformation (2.5) to formally express the beam deviation as a function of the rest-frame wavevector and wave frequency, giving

$$\begin{aligned}\tan\vartheta_t &= -\frac{\partial k_t^z}{\partial k_t^x} \\ &= -\left[\frac{\partial k_t^{z'}}{\partial k_t^{x'}}\frac{\partial k_t^{x'}}{\partial k_t^x} + \frac{\partial k_t^{z'}}{\partial \omega'}\frac{\partial \omega'}{\partial k_t^x}\right] \\ &= \gamma\left[v\frac{\partial k_t^{z'}}{\partial \omega'} - \frac{\partial k_t^{z'}}{\partial k_t^{x'}}\right].\end{aligned} \tag{3.7}$$

https://doi.org/10.1017/S0022377825000182 Published online by Cambridge University Press

Plugging in (3.4) then yields

$$\tan\vartheta_{t\alpha}=\gamma\left[v\frac{\partial\mathcal{K}'_\alpha}{\partial\omega'}(\omega',k_t^{x'})-\frac{\partial\mathcal{K}'_\alpha}{\partial k_t^{x'}}(\omega',k_t^{x'})\right], \tag{3.8}$$

where again ω' and $k_t^{x'}$ are given by (2.6*b*) and (2.2*a*).

In magnetised plasmas the dispersion relations are often expressed in terms of the components of the refractive index parallel and perpendicular to the background magnetic field $n_\parallel$ and $n_\perp$. Pursuing this analogy, we can similarly recast our results in terms of the refractive indexes parallel and perpendicular to the motion $n_t^{x'}=ck_t^{x'}/\omega'$ and $n_t^{z'}=\mathcal{N}'_\alpha=c\mathcal{K}'_\alpha/\omega'$, which leads to

$$\tan\theta_{t\alpha}=\frac{\sin\theta_i}{\mathcal{N}'_\alpha\left(\omega',n_t^{x'}\right)} \tag{3.9}$$

and

$$\tan\vartheta_\alpha=\gamma\left[\beta\left(\mathcal{N}'_\alpha(\omega',n_t^{x'})+\omega'\frac{\partial\mathcal{N}'_\alpha}{\partial\omega'}(\omega',n_t^{x'})\right)-\frac{\partial\mathcal{N}'_\alpha}{\partial n_t^{x'}}(\omega',n_t^{x'})\right], \tag{3.10}$$

where now

$$n_t^{x'}=\frac{\sin\theta_i-\beta}{1-\beta\sin\theta_i}. \tag{3.11}$$

We note that in the particular case where the rest-frame refractive index $\bar{n}_\alpha$ does not depend on the propagation direction, as is notably the case for O-X and L-R modes in magnetised plasmas (Ginzburg 1964), (3.4) reduces to

$$\mathcal{K}'_\alpha(\omega',k_t^{x'})=\sqrt{\left(\frac{\omega'\bar{n}_\alpha(\omega')}{c}\right)^2-k_t^{x'2}}. \tag{3.12}$$

One verifies that plugging this result into (3.6) and (3.8) yields the laboratory-frame transmitted angles (2.8) and (2.9) of an isotropic medium with refractive index $\bar{n}_\alpha$. Drag phenomena for this particular mode thus manifest essentially as in an isotropic medium with the appropriate index.

4. Generalised Snell's laws in the laboratory frame

The derivation of drag phenomena proposed in §§ 2 and 3 followed the approach proposed by Player (1975), that is to say to derive laboratory-frame refraction properties from those determined in the medium rest frame. This is the path illustrated in blue in figure 3. A different approach consists of modelling the interface directly in the laboratory frame. Indeed, since the moving medium as seen from the laboratory frame appears to have been bestowed additional properties as a result of motion (for instance bianisotropy (Kong 2008) and spatial dispersion (Lopez 1997)), one can seek to recast these additional properties in the form of generalised reflection and refraction laws, which can then be directly applied in the laboratory frame (Pyati 1967; Kong & Cheng 1968; Mukherjee 1975; Huang 1994). This is the red path in figure 3. In this section we make a brief digression to present this second approach and underline the equivalence of the two approaches.

As we have seen in § 2, the relation for the tangential part of the refracted wavevector is entirely deduced from continuity at the interface. On the other hand,

https://doi.org/10.1017/S0022377825000182 Published online by Cambridge University Press

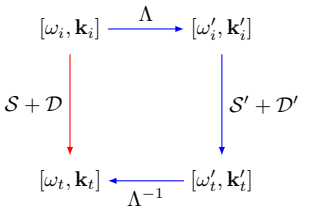


FIGURE 3. Representation of the two possible paths to derive the 4-wavevector of a beam refracted at the interface with a moving medium. The blue path represent the approach originally proposed by Player (1975), which uses standard refraction laws written in the rest frame (see §§ 2 and 3). The red path directly employs generalised Snell's laws written in the laboratory frame, in which motion appears as an effective property.

determining its normal component demands the dispersion function for the wave in the medium. Generalising this to the laboratory frame thus entails determining an effective dispersion function $\mathcal{D}(\omega, \mathbf{k})$, that is, the dispersion function that characterises wave propagation as seen in the laboratory frame. This is simply a generalisation of the previously defined rest-frame dispersion function (3.1). Here we use the result derived by Censor (1980) that the dispersion relations of any linear medium are covariant between inertial frames. This means that $\mathcal{D}(\omega, \mathbf{k})$ can simply be obtained by substituting to $\mathbf{k}'$ and ω' in $\mathcal{D}'(\omega', \mathbf{k}')$ their Lorentz transformation in the laboratory frame, or mathematically

$$\mathcal{D}(\omega, \mathbf{k}) = \mathcal{D}'\big(\omega'[\omega, \mathbf{k}], \mathbf{k}'[\omega, \mathbf{k}]\big). \tag{4.1}$$

Given this laboratory-frame dispersion function, Snell's law for the normal component of the wavevector is then written

$$k_t^z = \mathcal{K}(\omega_t, k_t^x), \tag{4.2}$$

where $\mathcal{K}$ is similarly the analogue of $\mathcal{K}'$ in (3.4). The generalised Snell's laws ($\mathcal{S}$) in the laboratory frame are thus written

$$\omega_t = \omega, \tag{4.3a}$$
$$k_t^x = k_i^x, \tag{4.3b}$$
$$k_t^z = \mathcal{K}(\omega_t, k_t^x). \tag{4.3c}$$

Since the equivalence of the two methods has already been demonstrated for the tangential part of the wavevector, all that is left to do is to verify the consistency of the two methods for the normal component of the wavevector, that is, (4.3*c*). Going back to our rest-frame analysis, the rest-frame refracted wavevector $\mathbf{k}_t'$ verifies the rest-frame dispersion relation, that is,

$$\mathcal{D}'\left(\omega_t', k_t^{x\prime}, k_t^{z\prime} = \mathcal{K}'(\omega_t', k_t^{x\prime})\right) = 0. \tag{4.4}$$

Meanwhile, substituting the laboratory-frame Lorentz transformation variables, and noting importantly that the normal component of the wavevector is unaffected $k_t^z = k_t^{z\prime}$, one can write

$$\begin{aligned}\mathcal{D}'\left(\omega_t', k_t^{x\prime}, k_t^{z\prime} = \mathcal{K}'(\omega_t', k_t^{x\prime})\right) &= \mathcal{D}'\left(\omega_t'[\omega_t, k_t^x], k_t^{x\prime}[\omega_t, k_t^x], k_t^{z\prime} = k_t^z\right) \\ &= \mathcal{D}\left(\omega_t, k_t^x, k_t^z\right). \end{aligned} \tag{4.5}$$

https://doi.org/10.1017/S0022377825000182 Published online by Cambridge University Press

Putting together (4.4) and (4.5), this implies that k_t^z verifies the dispersion relation in the laboratory frame, or in other words that $k_t^z = \mathcal{K}(\omega_t, k_t^x)$, which is precisely (4.3*c*). The two methods, as illustrated in blue and red in figure 3, are thus indeed equivalent.

To summarise, for a medium with known rest-frame dispersion function $\mathcal{D}'(\omega', \mathbf{k}')$, the covariance of the dispersion function demonstrated by Censor (1980) can be used to obtain the refracted wavevector directly in the laboratory frame. This result is consistent with the rest-frame approach proposed by Player (1975) and used above in §§ 2 and 3.

5. Application to moving magnetised plasmas

With the theory for the drag induced by a moving anisotropic medium in hand, we can now examine more particularly how these effects manifest themselves in a magnetised plasma in uniform linear motion with respect to the observer. We consider first these effects for the ordinary and extraordinary modes classically obtained for propagation perpendicular to the magnetic field, as the collinearity of rest-frame phase and group velocities (Ginzburg 1964) simplifies the algebra. In doing so, we recover previously established results, but also underline the important contribution of dispersion and Doppler shift to dragging effects. We then examine the more general case, making full use of the results from § 3.

5.1. *Magnetic field normal to the incidence plane (O and X modes)*

We consider here the moving medium to be a magnetised plasma with background magnetic field $\mathbf{B}_0' = B_0'\hat{\mathbf{y}}$ in its rest frame. Given our choice to have the incident wavevector $\mathbf{k}_i$ in the $(O, \hat{\mathbf{x}}, \hat{\mathbf{z}})$ plane, and the result that the Lorentz-transformed $\mathbf{k}_i'$ for $\mathbf{v} = v\hat{\mathbf{x}}$ is also in the $(O, \hat{\mathbf{x}}, \hat{\mathbf{z}})$ plane, this corresponds as shown in figure 4 to perpendicular propagation in the rest frame Σ'. The normal modes are hence classically the ordinary (O) and extraordinary (X) waves (Rax 2005, p. 288). We note that given the Lorentz transformations of fields

$$\mathbf{E}_\parallel = \mathbf{E}_\parallel', \tag{5.1a}$$

$$\mathbf{B}_\parallel = \mathbf{B}_\parallel', \tag{5.1b}$$

$$\mathbf{E}_\perp = \gamma\left(\mathbf{E}_\perp' - \mathbf{v}\times\mathbf{B}'\right), \tag{5.1c}$$

$$\mathbf{B}_\perp = \gamma\left(\mathbf{B}_\perp' + \mathbf{v}/c^2\times\mathbf{E}'\right), \tag{5.1d}$$

this field configuration implies $\mathbf{B}_0 = \gamma\mathbf{B}_0' \sim \mathbf{B}_0'$ and $\mathbf{E}_0 = -\mathbf{v}\times\mathbf{B}_0$ in the laboratory frame. This laboratory-frame field configuration $(\mathbf{E}_0, \mathbf{B}_0)$ is consistent with a plasma drift with velocity $\mathbf{v}$.

5.1.1. The O-mode

The refractive index of the O-mode in the rest frame, whose polarisation is along the magnetic field $\mathbf{B}_0'$, is simply written as

$$\bar{n}_{\mathrm{O}}(\omega') = \sqrt{1 - \left(\frac{\omega_p'}{\omega'}\right)^2}, \tag{5.2}$$

https://doi.org/10.1017/S0022377825000182 Published online by Cambridge University Press

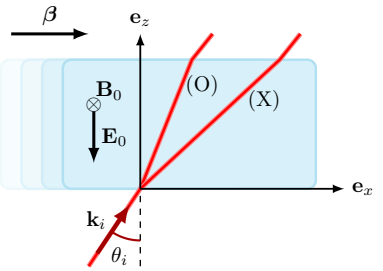


FIGURE 4. The incident wave is in the plane normal to the background magnetic field permeating the magnetised plasma in uniform linear motion. The rest-frame modes are the classical ordinary (O) and extraordinary (X) waves.

where $\omega_p'^2 = \sum_s \omega_{ps}'^2 = \sum_s n_s' e^2/(m_s'\epsilon_0)$ is the rest-frame plasma frequency. The associated dispersion function is

$$\mathcal{D}_{\mathrm{O}}'(\omega', \mathbf{k}') = \omega'^2 - k'^2c^2 - \omega_p'^2, \tag{5.3}$$

which, noting that the plasma frequency is Lorentz-invariant $\omega_p = \omega_p'$ (Chawla & Unz 1966), can be rewritten using the Lorentz transformation for ω' and $\mathbf{k}'$ as the laboratory-frame dispersion function

$$\mathcal{D}_{\mathrm{O}}(\omega, \mathbf{k}) = \omega^2 - k^2c^2 - \omega_p^2. \tag{5.4}$$

Comparing (5.3) and (5.4) shows that the O-mode dispersion relation is remarkably Lorentz-invariant. As a consequence, as noticed by Mukherjee (1975) and Ko & Chuang (1978), it is unaffected by motion. This property, which is characteristic of modes satisfying $\bar{n}\bar{n}_g = 1$, was suggested to support Minkowski's formulation of momentum partitioning in a medium (Arnaud 1976; Jones 1978). In this case the relations at the interface simply follow the static Snell's laws. One indeed finds plugging the mode's refractive index (5.2) into (3.9)–(3.10) that $\bar{n}_{\mathrm{O}} \sin\theta_t = \sin\theta_i$ and $\vartheta_t = \theta_t$, that is to say that the group velocity remains aligned with the wavevector in the laboratory frame.

5.1.2. The X-mode

The dispersion relation of the X-mode, whose polarisation is in the $(\mathbf{v}, \mathbf{k}')$ plane perpendicular to $\mathbf{B}_0'$, is written (Rax 2005, p. 289)

$$\bar{n}_{\mathrm{X}}(\omega') = \sqrt{\frac{(\omega'^2 - \omega_{\mathrm{L}}'^2)(\omega'^2 - \omega_{\mathrm{R}}'^2)}{(\omega'^2 - \omega_{\mathrm{UH}}'^2)(\omega'^2 - \omega_{\mathrm{LH}}'^2)}}, \tag{5.5a}$$

where

$$\omega_{\mathrm{R/L}}' = \mp\frac{\Omega_{ce}' + \Omega_{ci}'}{2} + \frac{1}{2}\sqrt{(\Omega_{ce}' - \Omega_{ci}')^2 + 4\omega_p'^2} \tag{5.5b}$$

are the right and left cutoffs and

$$\omega_{\mathrm{UH/LH}}' = \left[\frac{\varpi_e'^2 + \varpi_i'^2}{2} \pm \frac{1}{2}\sqrt{(\varpi_e'^2 - \varpi_i'^2)^2 + 4\omega_{pe}'^2\omega_{pi}'^2}\right]^{1/2} \tag{5.5c}$$

https://doi.org/10.1017/S0022377825000182 Published online by Cambridge University Press

are the upper- and lower-hybrid frequencies, and where we write $\varpi_s'^2 = \omega_{ps}'^2 + \Omega_{cs}'^2$ with $\Omega_{cs}' = q_s B_0'/m_s'$ the signed rest-frame cyclotron frequency for species s. One verifies that $\bar{n}\bar{n}_g \neq 1$, so that the X-mode is expected to experience Fresnel drag.

Asymptotic trends. Since the wave index (5.5*a*) does not depend on the incidence angle θ_i, drag phenomena for the X-mode can still, as already indicated above, be evaluated with the comparatively simpler isotropic model presented in § 2. Specifically plugging (5.5*a*) into (2.8)–(2.9) yields lengthy yet analytical formulae for the refraction and group velocity angles for any laboratory-frame wave frequency ω. As is customary, simpler forms can, however, be obtained if considering separately different wave frequency bands. For instance, if one focuses on the high-frequency electronic response, the wave index reduces to

$$\bar{n}_{\mathrm{X}}(\omega' \gg \omega_{\mathrm{LH}}') \sim \sqrt{1 - \frac{\omega_{pe}'^2(\omega'^2 - \omega_{pe}'^2)}{\omega'^2(\omega'^2 - \omega_{pe}'^2 - \Omega_{ce}'^2)}}. \tag{5.6}$$

In this limit (2.8), combined with the trigonometric relation $\sin\theta = \tan\theta/\sqrt{1+\tan^2\theta}$ and $\Omega_{cs} = \Omega_{cs}'/\gamma$ here, gives

$$\sin\theta_t = \sin\theta_i \left[1 - \frac{\omega_{pe}^2}{\omega^2} \frac{(1-\beta^2)\omega_{pe}^2 - (1-\beta\sin\theta_i)^2\omega^2}{\Omega_{ce}^2 + (1-\beta^2)\omega_{pe}^2 - (1-\beta\sin\theta_i)^2\omega^2}\right]^{-1/2} \tag{5.7}$$

which we verify is precisely the generalised Snell's law derived by Mukherjee (1975). Furthermore, using this same high-frequency wave index in the relation for the group velocity (2.9) in the limit of normal incidence $\theta_i = 0$ leads to

$$\tan\vartheta_t = \frac{\beta\gamma\omega_{pe}^2\Omega_{ce}^2}{\sqrt{[\omega^2 - \omega_{pe}^2/\gamma^2 - \Omega_{ce}^2]^3[(1-\omega_{pe}^2/\omega^2)(\gamma^2\omega^2 - \omega_{pe}^2) - \gamma^2\Omega_{ce}^2]}}, \tag{5.8}$$

which we verify is the result derived by Meyer-Vernet (1980). At very high frequency $\omega \gg \omega_{pe}, \Omega_{ce}$, $\tan\vartheta_t \propto \beta/(\gamma^2\omega^4)$. The drag is hence very small short of relativistic velocities.

The low-frequency regime $\omega' \leqslant \omega_{\mathrm{LH}}'$ has in contrast to our knowledge received less attention. In the limit $\omega' \leqslant \Omega_{ci}'$ and assuming $v_{\mathrm{A}}'/c = \Omega_{ci}'/\omega_{pi}' \ll 1$ with v_{A}' the Alfvén velocity, one classically shows that

$$\bar{n}_{\mathrm{X}}(\omega' \leqslant \omega_{\mathrm{LH}}') \sim \frac{c}{v_{\mathrm{A}}'}\sqrt{1 - \left(\frac{\omega'}{\Omega_{ci}'}\right)^2}. \tag{5.9}$$

Equation (2.9) then gives in the very-low-frequency regime $\omega' \ll \Omega_{ci}'$ and for normal incidence

$$\tan\vartheta_t = \frac{v}{v_{\mathrm{A}}} \tag{5.10}$$

to lowest order in β. This shows that, in contrast with the high-frequency regime, non-negligible drag can occur for the compressional Alfvén (or fast magnetoacoustic) branch of the X-mode, and that even for non-relativistic velocities.

To confirm these trends, explore the intermediate-frequency regimes and study the effect of incidence, we now examine the results obtained using the full solution

https://doi.org/10.1017/S0022377825000182 Published online by Cambridge University Press

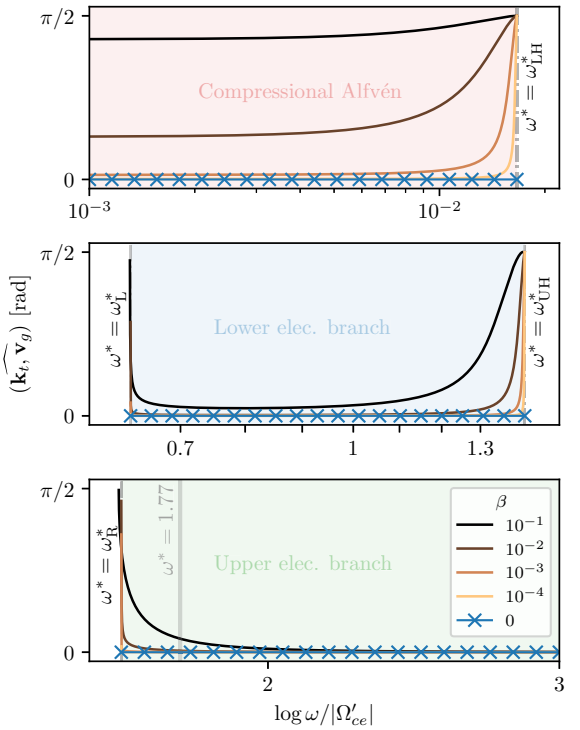


FIGURE 5. Angle between the group velocity $\mathbf{v}_g$ and the wavevector $\mathbf{k}_t$ of the X-mode refracted by a wave at normal incidence on a moving magnetised plasma, as a function of the frequency and for several values of the velocity, for a hydrogen plasma with $n'_e = 10^{19}$ m^{-3} and $B'_0 =$ 1 T. Here $(\mathbf{v}, \mathbf{k}_t, \mathbf{B}_0)$ forms an orthogonal basis. The three panels represent the three standard propagation branches of the X-mode. The superscript * indicates a normalisation by the rest-frame electron cyclotron frequency $|\Omega'_{ce}|$. The vertical grey line for $\omega^* = 1.77$ in the third panel highlights the frequency for which oblique incidence is examined in figure 6.

(5.5*a*) in (2.8)–(2.9). To this end we consider as a baseline a hydrogen plasma with density $n'_e = 10^{19}$ m^{-3} and rest-frame magnetic field $B'_0 = 1$ T.

Normal incidence. To start with, we consider the case of normal incidence, that is, when $(\mathbf{v}, \mathbf{B_0}', \mathbf{k}_i)$ forms an orthogonal basis. In this particular case the transmitted wavevector $\mathbf{k}_t$ is conveniently along $\mathbf{k}_i$, i.e. along $\hat{\mathbf{z}}$. Figure 5 plots the angle $(\widehat{\mathbf{k}_t, \mathbf{v}_g})$ between the refracted wavevector $\mathbf{k}_t$ and the group velocity $\mathbf{v}_g$ across the entire frequency range for different values of $\beta = v/c$. Without motion, i.e. for $\beta = 0$, we recover the classical behaviour of the X-mode, that is to say a group velocity that is aligned with the wavevector $\mathbf{v}_g \parallel \mathbf{k}$. This materialises in figure 5 as an angle $(\widehat{\mathbf{k}_t, \mathbf{v}_g})$ that is zero for all frequencies. We also recognise in figure 5 for $\beta = 0$ the three usual propagation branches of this mode, namely below the lower-hybrid resonance ω_{LH}, in between the left cutoff ω_{L} and the upper-hybrid resonance ω_{UH}, and finally above the right cutoff ω_{R} (Rax 2005, p. 289).

Moving on to the effect of velocity, figure 5 confirms that the angle $(\widehat{\mathbf{k}_t, \mathbf{v}_g})$ is now finite for $\beta \neq 0$, and positive for all frequencies. This means that the X-mode is dragged in the direction of motion. This drag is further found to increase with velocity for all frequencies. Overall, drag effects are observed to be strongly enhanced

https://doi.org/10.1017/S0022377825000182 Published online by Cambridge University Press

near resonances and cutoffs. They even reach at these frequencies the maximum angle $\pi/2$ which represents a limit case where the wave is fully dragged by the medium. Although this increase appears consistent with the classic $\bar{n}_g - 1/\bar{n}$ scaling of transverse drag (Player 1975) (the phase velocity goes to zero near cutoffs while the group velocity goes to infinity near resonances) and with the observation of enhanced drag effects in slow-light media (Franke-Arnold *et al.* 2011), results for these frequencies warrant caution as the cold plasma model used in this study is expected to break down. Notwithstanding these limitations, these results suggest that augmented drag effects could be achieved near resonances and cutoffs.

Away from resonances and cutoffs, figure 5 confirms that drag effects are negligible for the two high-frequency bands, consistent with (5.8). On the other hand, figure 5 also confirms that significant drag occurs at low frequency $\omega \leqslant \omega_{\rm LH}$ as anticipated from (5.10). In this low-frequency regime the angle $(\widehat{\mathbf{k}_t, \mathbf{v}_g})$ is observed to be nearly independent of the wave frequency, consistent with the fact that the X-mode at these frequencies is nearly non-dispersive. Quantitatively, we find a drag of a few degrees for $\beta \sim 10^{-4}$. This result matches the prediction from (5.10) as $c/v_A \sim 40$ for the plasma parameters considered here, and larger drags are expected for denser plasmas at the same field (or a similar density but at weaker fields).

Oblique incidence and Doppler. While the low-frequency X-mode is nearly non-dispersive, this is not the case at higher frequency, which brings additional complexity. More precisely, dispersion can manifests due to the Doppler shift experienced by the wave as seen in the rest frame, leading to new effects compared with the non-dispersive medium considered in § 2. Specifically, the Lorentz transformation for the wave frequency (2.2*a*) shows that the rest-frame frequency ω' depends on the angle of incidence θ_i. As a result, the propagation bands of the X-mode, which normally are independent of the wavevector direction, now depend on the incidence angle θ_i.

To illustrate this point, we have plotted in figure 6 the refraction diagrams obtained for the X-mode with normalised rest-frame wave frequency $\omega^* = \omega/|\Omega'_{ce}| = 1.77$. As shown in figure 5 this frequency falls in the high-frequency electronic branch of the X-mode for $\beta = 0$, just above the right cutoff. We see in figure 6 that while the effect of motion is limited at low β, new features emerge for larger β. It is notably found that the incident wave, which again verifies $\omega > \omega_{\rm R}$, can in fact couple instead to the low-frequency electronic branch for sufficiently large β and k_i^x (i.e. sufficiently large incidence angle θ_i). For $k_i^x > 0$ the Doppler shift is indeed such that $\omega' < \omega$, and ω' can become smaller than the rest-frame upper-hybrid frequency $\omega'_{\rm UH}$. In this case a strong drag is observed, as ω' is close to the resonance. As a direct consequence of this behaviour, we note the existence of an intermediate total reflection region in between the values of k_i^x yielding these two distinct branches. This remarkable feature is entirely due to the plasma motion. Note also that a symmetrical behaviour can be observed if choosing a rest-frame frequency in the low-frequency electronic branch just below the upper-hybrid resonance, and this time $k_i^x < 0$ so that $\omega' > \omega$.

To sum up, it is found here that while drag effects on the X-mode are generally small at high frequency away from cutoffs and resonances, they can be significant at low frequency, i.e. for the compressional Alfvén branch. In addition, the motion can have a noticeable effect near resonances and cutoffs, where it can lead to jumps from a given branch to the other as the incidence angle changes at fixed wave frequency, to the onset of incidence-angle-dependent asymmetric propagation windows and also possibly to augmented drag effects.

https://doi.org/10.1017/S0022377825000182 Published online by Cambridge University Press

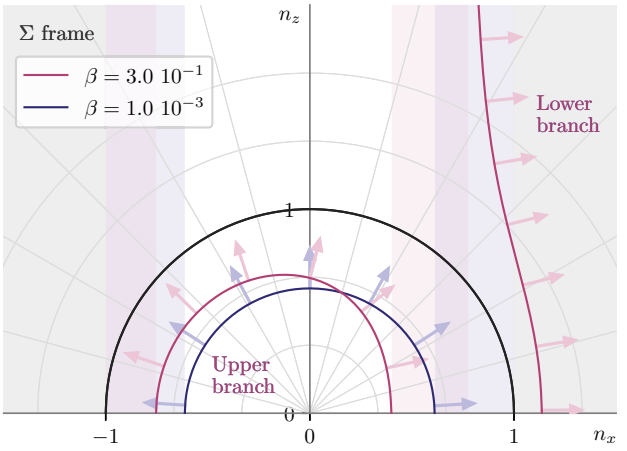


FIGURE 6. Refraction diagrams for a wave with rest-frame right cutoff ($\omega/|\Omega'_{ce}| = 1.77$) at oblique incidence on a moving plasma for two different values of β. In the absence of motion the refracted wave is on the upper branch of the X-mode. The coloured bands highlight the regions of total reflection.

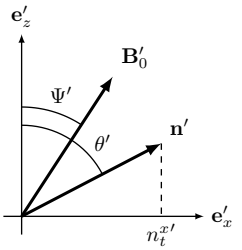


FIGURE 7. Configuration with the rest-frame magnetic field $\mathbf{B}'_0$ in the plane defined by the incident wavevector $\mathbf{k}_i$ and the medium velocity $\mathbf{v}$. Propagation is in this case in general oblique.

5.2. *Magnetic field in the incidence plane*

To expose how rest-frame anisotropy can further complicate the drag picture, we finally consider the case where the magnetic field $\mathbf{B}'_0$ lies in the plane defined by the incident wavevector $\mathbf{k}_i$ and the medium velocity $\mathbf{v}$. As depicted in figure 7, we write Ψ' as the angle in this plane between the normal to the velocity and the magnetic field. Other than for singular values of Ψ' the wavevector is now inclined with respect to the rest-frame magnetic field, so that the rest-frame indexes $\bar{n}'_\alpha$ indeed depend on the wavevector of the refracted wave $\mathbf{k}'_t$, i.e. on the propagation direction in the rest frame.

5.2.1. General formulation

Propagation in the rest frame is oblique, and as such is governed by a generalised Appleton–Hartree equation (Bittencourt 2013). The normal component of the wave index $\mathcal{N}'$ (3.10) can then be shown to verify the quartic equation

$$\Lambda\mathcal{N}'^4 + \Theta\mathcal{N}'^3 + \Gamma\mathcal{N}'^2 + \Upsilon\mathcal{N}' + \Xi = 0 \tag{5.11}$$

https://doi.org/10.1017/S0022377825000182 Published online by Cambridge University Press

with

$$\Lambda = P\cos^2(\Psi') + S\sin^2(\Psi'), \tag{5.12a}$$

$$\Theta = n_t^{x'}\sin(2\Psi')(P-S), \tag{5.12b}$$

$$\Gamma = \left[\cos(2\Psi')(LR-PS) - LR + 2n_t^{x'2}(P+S) - 3PS\right]/2, \tag{5.12c}$$

$$\Upsilon = n_t^{x'}\sin(2\Psi')\left[LR + n_t^{x'2}(P-S) - PS\right]/2, \tag{5.12d}$$

$$\Xi = P\left[n_t^{x'2}\sin^2(\Psi')(n_t^{x'2}-S) + LR - n_t^{x'2}S\right] + n_t^{x'2}\cos^2(\Psi')(n_t^{x'2}S - LR), \tag{5.12e}$$

where $n_t^{x'} = k_t^{x'}c/\omega'$ and P, L, R, S are the classical functions defined by Stix (1992). They here depend on the rest-frame frequency ω' and are explicitly written as

$$P(\omega') = 1 - \sum_s \frac{\omega_{ps}^2}{\omega'^2}, \tag{5.13a}$$

$$R(\omega') = 1 - \sum_s \frac{\omega_{ps}^2}{\omega'(\omega'+\Omega'_{cs})}, \qquad L(\omega') = 1 - \sum_s \frac{\omega_{ps}^2}{\omega'(\omega'-\Omega'_{cs})} \tag{5.13b}$$

and

$$S(\omega') = \frac{1}{2}(R+L) = 1 - \sum_s \frac{\omega_{ps}^2}{\omega'^2 - \Omega_{cs}'^2}. \tag{5.13c}$$

Compared with standard textbook expressions, the odd terms in (5.11) are here non-zero because the background magnetic field $\mathbf{B}'_0$ is not aligned with a basis vector in Σ'. Nonetheless, the quartic equation (5.11) must similarly yield two modes that are either purely propagative ($\mathcal{N}' > 0$) or evanescent ($\mathcal{N}'^2 < 0$), as usual in a magnetised plasma. Although cumbersome, this quartic equation (5.11) can be solved to obtain the index $\mathcal{N}'_\pm$ of these two modes, denoted here by the subscript $\pm$. These wave indexes can then be used to compute the drag experienced by each of the beams using (3.10).

5.2.2. Magnetic field along the direction of motion

Rather than going this route, we focus here on the particular case $\Psi' = \pi/2$, that is to say on the case where the magnetic field is parallel to the direction of motion $\mathbf{v}$. We note that this configuration, which is illustrated in figure 8, could for instance be thought of as a simplified model for the effect of toroidal rotation in a tokamak. In this case (5.12) then gives $\Theta = \Upsilon = 0$, so that the Appleton equation (5.11) reduces to the more usual bi-quadratic equation

$$\Lambda_\parallel \mathcal{N}'^4 + \Gamma_\parallel \mathcal{N}'^2 + \Xi_\parallel = 0, \tag{5.14a}$$

where

$$\Lambda_\parallel = S, \tag{5.14b}$$

$$\Gamma_\parallel = n_t^{x'2}(P+S) - (LR+PS), \tag{5.14c}$$

$$\Xi_\parallel = P(n_t^{x'2} - L)(n_t^{x'2} - R). \tag{5.14d}$$

https://doi.org/10.1017/S0022377825000182 Published online by Cambridge University Press

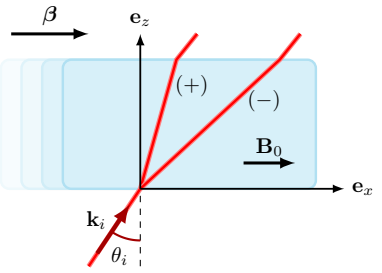


FIGURE 8. The incident wave is in the plane formed by the background magnetic field $\mathbf{B}_0' = \mathbf{B}_0$ permeating the magnetised plasma and the direction of motion $\boldsymbol{\beta}$. The rest-frame modes are the two solutions (+) and (−) for oblique propagation.

As expected the odd terms are here zero as $\mathbf{B}_0'$ is now along $\hat{\mathbf{x}}$. Also, from the Lorentz transformations of fields (5.1), the laboratory-frame electric field is null, and the external magnetic field is the same in the laboratory frame and in the rest frame, i.e. $\mathbf{B}_0 = \mathbf{B}_0'$. As a result the prime on the cyclotron frequencies can be dropped in (5.13).

Although $\bar{n}_\alpha'$ still depend on the wavevector of the refracted wave $\mathbf{k}_t'$ since $\mathbf{k}_t'$ is in general inclined with respect to $\mathbf{B}_0'$, this bi-quadratic equation has, compared with (5.11), simpler analytical solutions in the form of

$$\mathcal{N}_\pm' = \left[\frac{1}{2\Lambda_\parallel}\left(-\Gamma_\parallel \pm \sqrt{\Gamma_\parallel^2 - 4\Lambda_\parallel \Xi_\parallel}\right)\right]^{1/2}. \tag{5.15}$$

The two modes denoted here by (+) and (−) are the standard solutions for oblique propagation, also referred to as the slow and fast modes, respectively. In the particular case of normal incidence for which $\mathbf{k}_t' \perp \mathbf{B}_0'$, the (+) or slow solution is found to reduce to the O-mode, whereas the (−) or fast solution reduces to the X-mode. These general solutions (5.15) can then be used in (3.10) to derive explicit formulas for the Fresnel drag.

To illustrate how drag effects and rest-frame anisotropy can compete with one another, figure 9 plots on the left-hand side the same angle $(\widehat{\mathbf{k}_t, \mathbf{v}_g})$ as in figure 5, but we consider now the (−) mode at finite incidence angle $\theta_i = -\pi/4$. We focus here on the low-frequency branch. For frequencies just above the ion cyclotron frequency, we observe a behaviour similar to that of the compressional Alfvén branch at normal incidence already observed in figure 5, that is, a drag in the direction of motion that increases with the velocity, and that can be significant even for modest β. This similarity can be explained as follows. For $\omega' \sim \Omega_{ci}$ one shows that the axial wave index $\mathcal{N}_-'$ is large for as long as

$$n_t^{x'} \ll \sqrt{R} \sim \frac{\omega_{pi}}{\sqrt{2}\Omega_{ci}}, \tag{5.16}$$

reaching

$$\mathcal{N}_-' \sim \sqrt{\frac{LR}{S}} \sim \frac{\omega_{pi}}{\Omega_{ci}} \tag{5.17}$$

for perpendicular propagation $n_t^{x'} = 0$. This is verified in the dispersion diagram on the right-hand side of figure 9. Since $n_t^{x'} \leqslant 1$ from (2.3*b*), this shows that the rest-frame refractive index will be large, which from Snell's law implies that the refracted

https://doi.org/10.1017/S0022377825000182 Published online by Cambridge University Press

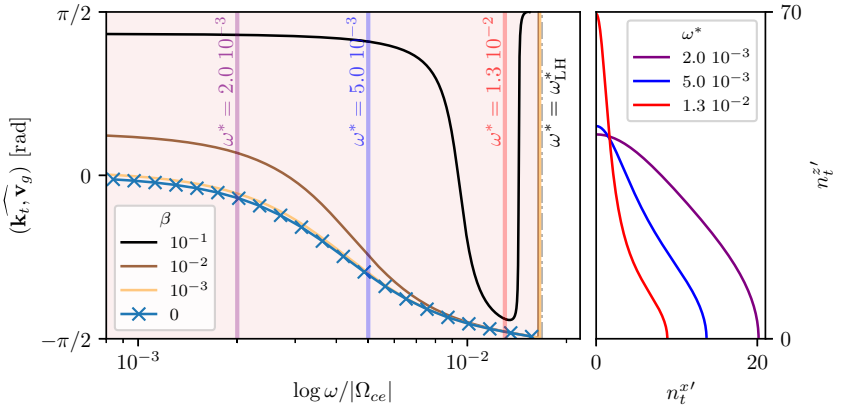


FIGURE 9. Angle between the transmitted group velocity $\mathbf{v}_g$ and the wavevector $\mathbf{k}_t$ as a function of the frequency for a $(-)$ mode incident with $\theta_i = -45°$ for different values of the velocity (left), and rest-frame dispersion diagram $(n_t^{x'}, n_t^{z'})$ for the three wave frequencies highlighted on the left-hand side (right). The region of interest here is in between the ion cyclotron frequency $(\Omega_{ci}/|\Omega_{ce}| = 5.4 \times 10^{-4})$ and the lower-hybrid frequency $(\omega_{\mathrm{LH}}/|\Omega_{ce}| = 1.7 \times 10^{-2})$. The plasma parameters are those already used in figure 5, leading to $c/v_A = 43.4$.

wavevector $\mathbf{k}'_t$ is close to $\hat{\mathbf{z}}$. This in turn implies nearly perpendicular propagation in Σ', thus the X-mode-like behaviour.

As the frequency increases, however, we observe a departure from this behaviour, with the angle $\widehat{(\mathbf{k}_t, \mathbf{v}_g)}$ that now decreases with frequency. It notably becomes negative for large enough frequency, and even for significant β. Because the rest-frame refractive index remains large (see the right-hand side of figure 9), it implies that the component of the group velocity along $\mathbf{v}$ must now be negative. The reason for that, as supported by the curve obtained for $\beta = 0$ in figure 9, is the rest-frame anisotropy. Indeed, the angle between $\mathbf{k}'_t$ and $\mathbf{v}'_g$ grows and approaches $-\pi/2$ at the lower-hybrid resonance. We see in figure 9 that, short of very large β, the anisotropy progressively suppresses drag effects in the frequency range below the lower-hybrid frequency. Yet, drag effects eventually dominate again in the immediate vicinity of the cutoff, as the group index goes to infinity at the resonance. This translates into a sudden π upshift near $\omega = \omega_{\mathrm{LH}}$ in figure 9.

For completeness, we note here (not shown in figure 9) that a behaviour similar to that discussed earlier for the X-mode, notably enhanced drag and dispersion effects near high frequency cutoffs and resonances (electron cyclotron range), is also observed in this configuration.

In summary, rest-frame anisotropy is found to bring about additional complexity on top of the motion drag effects already identified for the X-mode. These two effects can notably oppose one another, with a relative importance that depends strongly on the wave frequency. More practically, the fact that these results are obtained for a configuration which, while very simplified, in essence matches that of a toroidal flow in a tokamak, and for a wave frequency range relevant to magnetic confinement fusion applications, points to the need to explore these manifestations further.

https://doi.org/10.1017/S0022377825000182 Published online by Cambridge University Press

6. Conclusions

The transmission angles for the wavevector and the group velocity of a wave at oblique incidence on an anisotropic medium in uniform linear motion directed along the interface, as observed by an observer in the laboratory frame, have been determined analytically. These findings confirm and extend results that had been previously established, notably for isotropic media and/or for normal incidence.

These laboratory-frame relations for the wavevector and group velocity, which were obtained by considering Snell's law in the reference frame in which the anisotropic medium is at rest, are further shown to be consistent with the generalised Snell's law. More specifically, the interface relations derived here match Snell's law written for the rest-frame index one obtains by invoking the covariance of the dispersion relation between inertial frames. In doing so one can then retire the need for the change of frame of reference in determining the laboratory-frame relations, by considering instead the moving medium has an equivalent medium bestowed with motion-dependent properties. This direct method may, however, come at the expense of physical insights.

These new results were then applied to examine the effect of motion on waves incident on a magnetised plasma in uniform linear motion. Starting with the simpler case where the magnetic field is normal to the incident wavevector, for which the rest-frame wavevector and group velocity of the refracted wave are aligned, we show that while the O-mode is unaffected by the motion, the motion can in contrast affect the X-mode. While, as previously noticed, drag effects are weak at high frequency, it is found here that they could be significant for the low-frequency compressional Alfvén branch. Motion, through the Doppler shift experienced by the wave, is also found to create asymmetric total reflection conditions, and even incidence-angle-dependent propagation bands near cutoffs and resonances.

We finally considered the case where the magnetic field is aligned with the medium's direction of motion, for which the rest-frame wavevector and group velocity of the refracted wave are no longer aligned. While very simplified, this configuration shares similarities with the geometry of a wave incident on a toroidally rotating tokamak plasma. In this case it is found that, in addition to the effects found for perpendicular propagation, anisotropy and drag can now compete with one another, notably near the lower-hybrid frequency.

Looking ahead, the finding that plasma motion can under certain conditions affect the trajectory of waves in possibly non-negligible ways, notably for wave frequencies below the electron cyclotron frequency, confirms that accounting for these effect could be important for the accurate modelling of radiofrequency waves in magnetic confinement fusion plasmas. With that in mind, a goal with these results in hand would be to quantify how large these motion-induced wave trajectory corrections are in practical configurations, similarly to what has been done for instance for the corrections due to spin–orbit coupling (Fu, Dodin & Qin 2023).

Acknowledgements

J.L. acknowledges the support of ENS Paris-Saclay through its Doctoral Grant Programme.

Funding

This work is supported by the Agence Nationale de la Recherche (ANR) through the WaRP project (ANR-21-CE30-0002). This work has been carried out within the

https://doi.org/10.1017/S0022377825000182 Published online by Cambridge University Press

framework of the EUROfusion Consortium, via the Euratom Research and Training Programme (grant agreement no. 101052200 – EUROfusion). Views and opinions expressed are, however, those of the authors only and do not necessarily reflect those of the European Union or the European Commission.

Declaration of interests

The authors report no conflict of interest.

REFERENCES

ARNAUD, J.A. 1976 Dispersion and the transverse aether drag. *Nature* **261** (5560), 481–482.

BITTENCOURT, J.A. 2013 *Fundamentals of Plasma Physics*. Springer Science & Business Media.

BOURGOIN, A., ZANNONI, M., GOMEZ CASAJUS, L., TORTORA, P. & TEYSSANDIER, P. 2021 Relativistic modeling of atmospheric occultations with time transfer functions. *Astron. Astrophys.* **648**, A46.

BOURGOIN, A., ZANNONI, M. & TORTORA, P. 2019 Analytical ray-tracing in planetary atmospheres. *Astron. Astrophys.* **624**, A41.

CARUSOTTO, I., ARTONI, M., ROCCA, G.C.L. & BASSANI, F. 2003 Transverse Fresnel-Fizeau drag effects in strongly dispersive media. *Phys. Rev. A* **68** (6), 063819.

CENSOR, D. 1980 Dispersion equations in moving media. *Proc. IEEE* **68** (4), 528–529.

CHAWLA, B.R. & UNZ, H. 1966 A note on the Lorentz transformations for a moving anisotropic plasma. *Radio Sci.* **1** (9), 1055–1055.

DECK-LÉGER, Z.-L., ZHENG, X. & CALOZ, C. 2021 Electromagnetic wave scattering from a moving medium with stationary interface across the interluminal regime. *Photonics* **8** (6), 202.

EINSTEIN, A. 1905 Zur elektrodynamik bewegter Körper. *Ann. Phys*. **17**, 891–921.

ENDRIZZI, D. *et al.*et al. 2023 Physics basis for the wisconsin hts axisymmetric mirror (wham). *J. Plasma Phys.* **89** (5), 975890501.

FERMI, E. 1923 Sul trascinamento del piano di polarizzazione da parte di un messo rotante. *Rend. Mat. Acc. Lincei* **32**, 115–118.

FETTERMAN, A.J. & FISCH, N.J. 2008 Alpha channeling in a rotating plasma. *Phys. Rev. Lett.* **101** (20), 205003.

FISCH, NATHANIEL J. 1987 Theory of current drive in plasmas. *Rev. Mod. Phys.* **59** (1), 175–234.

FIZEAU, H. 1851 Sur les hypothèses relatives à l'éther lumineux, et sur une expérience qui paraît démontrer que le mouvement des corps change la vitesse avec laquelle la lumière se propage dans leur intérieur. *C. R. Acad. Sci. Paris* **33**, 349–355.

FRANKE-ARNOLD, S., GIBSON, G., BOYD, R.W. & PADGETT, M.J. 2011 Rotary photon drag enhanced by a slow-light medium. *Science* **333** (6038), 65–67.

FRESNEL, A. 1818 Lettre d'Augustin fresnel à françois Arago sur l'influence du mouvement terrestre dans quelques phénomènes d'optique. *Ann. Chim. Phys.* **9**, 57–66.

FU, Y., DODIN, I.Y. & QIN, H. 2023 Spin hall effect of radiofrequency waves in magnetized plasmas. *Phys. Rev. E* **107** (5), 055210.

GINZBURG, V.L. 1964 *The Propagation Of Electromagnetic Waves In Plasmas*. Addison-Wesley, Reading, Mass.

GJURCHINOVSKI, A. 2004 Aberration of light in a uniformly moving optical medium. *Am. J. Phys.* **72** (7), 934–940.

GUEROULT, R., RAX, J.-M. & FISCH, N.J. 2020 Enhanced tuneable rotatory power in a rotating plasma. *Phys. Rev. E* **102** (5), 051202(R).

GUEROULT, R., RAX, J.-M. & FISCH, N.J. 2023 Wave propagation in rotating magnetised plasmas. *Plasma Phys. Control. Fusion* **65** (3), 034006.

GUEROULT, R., SHI, Y., RAX, J.-M. & FISCH, N.J. 2019 Determining the rotation direction in pulsars. *Nat. Commun.* **10** (1), 3232.

HUANG, YAO-XIONG 1994 Reflection and transmission of electromagnetic waves by a dielectric medium moving in an arbitrary direction. *J. Appl. Phys.* **76** (5), 2575–2581.

https://doi.org/10.1017/S0022377825000182 Published online by Cambridge University Press

JONES, R.V. 1975 Aether drag' in a transversely moving medium. *Proc. R. Soc. A* **345**(1642), 351–364.
JONES, R.V. 1976 Rotary aether drag. *Proc. R. Soc. A* **349**(1659), 423–439.
JONES, R.V. 1978 Radiation pressure of light in a dispersive medium. *Proc. R. Soc. Lond. A. Math. Phys. Sci.* **360**(1702), 365–371.
KO, H.C. & CHUANG, C.W. 1978 On the passage of radiation through moving astrophysical plasmas. *Astrophys. J.* **222**, 1012–1019.
KOLMES, E.J., OCHS, I.E., RAX, J.-M. & FISCH, N.J. 2024 Massive, long-lived electrostatic potentials in a rotating mirror plasma. *Nat. Commun.* **15** (1), 4302.
KONG, J.A. 1974 Optics of bianisotropic media. *J. Opt. Soc. Am.* **64** (10), 1304.
KONG, J.A. 2008 *Electromagnetic Wave Theory*. EMW Publishing.
KONG, J.-A. & CHENG, D.K. 1968 Wave behavior at an interface of a semi-infinite moving anisotropic medium. *J. Appl. Phys.* **39** (5), 2282–2286.
KRISHNAKUMAR, M.A. *et al.*et al. 2021 High precision measurements of interstellar dispersion measure with the upgraded gmrt. *Astron. Astrophys.* **651**, A5.
KUMAR, P., WHITE, S.M., STOVALL, K., DOWELL, J. & TAYLOR, G.B. 2022 Pulsar observations at low frequencies: applications to pulsar timing and solar wind models. *Mon. Not. R. Astron. Soc.* **511** (3), 3937–3950.
LANDAU, L.D. & LIFSCHITS, E.M. 1975 The classical theory of fields. In *Course of Theoretical Physics*, vol. **2**. Pergamon Press.
LEHNERT, B. 1971 Rotating plasmas. *Nucl. Fusion* **11** (5), 485–533.
LOPEZ, E. 1997 Dispersion of electromagnetic waves in active moving plasma. *Astron. Astrophys. Trans.* **14** (1), 79–85.
MEYER-VERNET, N. 1980 High-frequency transverse Fresnel drag in a moving magneto-active plasma. *Astrophys. Space Sci.* **73** (1), 207–212.
MUKHERJEE, P.K. 1975 Electromagnetic wave propagation in a moving magnetoplasma medium in the presence of a boundary. *J. Appl. Phys.* **46** (5), 2295–2297.
OCHS, I.E. 2024 When do waves drive plasma flows? *Phys. Plasmas* **31** (4), 042116.
OCHS, I.E. & FISCH, N.J. 2021*a* Nonresonant diffusion in alpha channeling. *Phys. Rev. Lett.* **127** (2), 025003.
OCHS, I.E. & FISCH, N.J. 2021b Wave-driven torques to drive current and rotation. *Phys. Plasmas* **28** (10), 102506.
OCHS, I.E. & FISCH, N.J. 2022 Momentum conservation in current drive and alpha-channeling-mediated rotation drive. *Phys. Plasmas* **29** (6), 062106.
PLAYER, M.A. 1975 Dispersion and the transverse aether drag. *Proc. R. Soc. A* **345**(1642), 343–344.
PLAYER, M.A. 1976 On the dragging of the plane of polarization of light propagating in a rotating medium. *Proc. R. Soc. A* **349** (1659), 441.
PRATER, R. *et al.*et al. 2008 Benchmarking of codes for electron cyclotron heating and electron cyclotron current drive under iter conditions. *Nucl. Fusion* **48** (3), 035006.
PYATI, V.P. 1967 Reflection and refraction of electromagnetic waves by a moving dielectric medium. *J. Appl. Phys.* **38** (2), 652–655.
RAX, J.-M. 2005 Physique des plasmas: cours et applications. *Dunod*.
RAX, J.-M., GUEROULT, R. & FISCH, N.J. 2023*a* Rotating alfvén waves in rotating plasmas. *J. Plasma Phys.* **89** (6), 905890613.
RAX, J.-M., GUEROULT, R. & FISCH, N.J. 2023*b* DC electric field generation and distribution in magnetized plasmas. *Phys. Plasmas* **30** (7), 072509.
RAX, J.-M., GUEROULT, R. & FISCH, N.J. 2023*c* Quasilinear theory of Brillouin resonances in rotating magnetized plasmas. *J. Plasma. Phys.* **89** (4), 905890408.
RUBIN, T., OCHS, I.E. & FISCH, N.J. 2024 Flowing plasma rearrangement in the presence of static perturbing fields. *Phys. Plasmas* **31** (8), 082109.
RUBIN, T., RAX, J.M. & FISCH, N.J. 2023 Magnetostatic ponderomotive potential in rotating plasma. *Phys. Plasmas* **30** (5), 052501.
RYBAK, J. & CHURCHILL, R.J. 1971 Progress in reentry communications. *IEEE Trans. Aerosp. Electron. Syst.* **AES-7** (5), 879–894.

https://doi.org/10.1017/S0022377825000182 Published online by Cambridge University Press

SEGRE, S.E. 1999 A review of plasma polarimetry - theory and methods. *Plasma Phys. Control. Fusion* **41** (2), R57–R100.

STARKEY, R.P. 2015 Hypersonic vehicle telemetry blackout analysis. *J. Spacecr. Rockets* **52** (2), 426–438.

STIX, T.H. 1992 *Waves in Plasmas*. Springer Science & Business Media.

VAN ECK, C.L. *et al.*et al. 2017 Faraday tomography of the local interstellar medium with Lofar: Galactic foregrounds towards ic 342. *Astron. Astrophys.* **597**, A98.

https://doi.org/10.1017/S0022377825000182 Published online by Cambridge University Press